Protein-based models offer mechanistic insight into complex nickel metalloenzymes

Regina E. Treviño and Hannah S. Shafaat*

Department of Chemistry and Biochemistry, The Ohio State University, Columbus, OH

Shafaat.1@osu.edu

Table of Contents Graphic

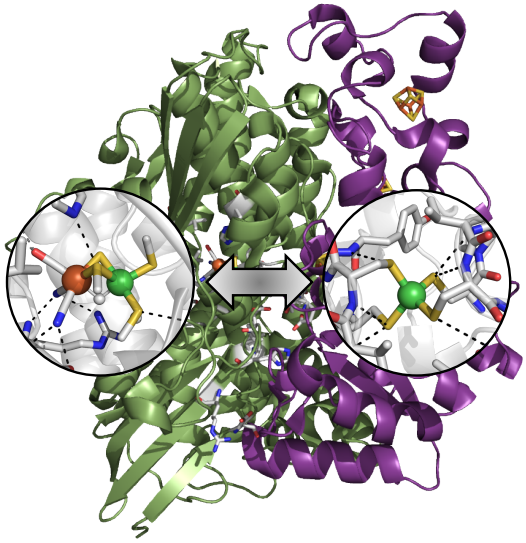

Abstract

There are ten nickel enzymes found across biological systems, each with a distinct active site and reactivity that spans reductive, oxidative, and redox-neutral processes. We focus on the reductive enzymes, which catalyze reactions that are highly germane to the modern-day climate crisis: [NiFe] hydrogenase, carbon monoxide dehydrogenase, acetyl coenzyme A synthase, and methyl coenzyme M reductase. The current mechanistic understanding of each enzyme system is reviewed along with existing knowledge gaps, which are addressed through the development of protein-derived models, as described here. This opinion is intended to highlight the advantages

of using robust protein scaffolds for modeling multiscale contributions to reactivity and inspire development of novel artificial metalloenzymes for other small molecule transformations.

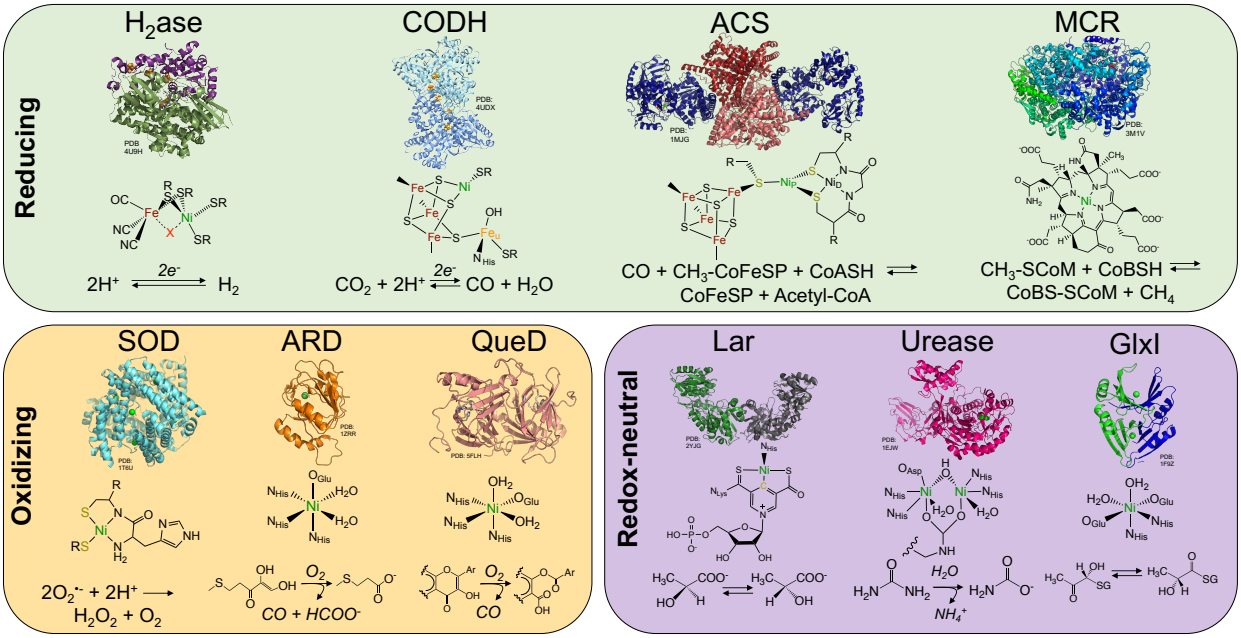

Figure 1. Protein architecture, active site structure, and reaction catalyzed for the ten known nickel metalloenzymes, divided by reactivity type.

Introduction

Nature showcases the versatility of nickel across the three kingdoms of life by incorporating this valuable metal ion within diverse enzymes. Of the ten nickel-containing enzymes identified to date, each features a unique protein architecture and distinct active site ligation (**Figure 1**).[1–11] The chemistry performed by these enzymes is highly varied, spanning redox-active reductive and oxidative processes as well as redox-neutral hydrolysis and isomerization reactions. While there is a plethora of interesting chemistry to be explored regarding the selection of nickel for each of these reactions, particularly with respect to the weak nickel-oxygen bonds that facilitate substrate transformation rather than degradative nickel oxidation in SOD, ARD, and QueD, this opinion will focus on the reductive nickel enzymes. The [NiFe] hydrogenase (H_2ase), carbon monoxide dehydrogenase (CODH), acetyl coenzyme A synthase (ACS) and methyl coenzyme M reductase (MCR) are considered champions of clean energy conversion, and three of these are heavily

involved in mediating global carbon gas cycles.[1] In this opinion, we emphasize key reactivity traits of the native nickel enzymes and describe recent advances in development of nickel-containing, protein-based models that offer insight into the enzymatic mechanisms. We anticipate this will highlight the advantages of using robust protein scaffolds for modeling multiscale contributions to reactivity and inspire development of novel artificial metalloenzymes for other small molecule transformations.

[NiFe] hydrogenases: Enzymatic control across length scales

The [NiFe] H_2ases feature highly complex active-site environments and conserved structural elements that work synergistically to enable rapid and efficient turnover. The primary coordination sphere of the enzyme has a heterobimetallic [NiFe] site, with the atoms bridged by two cysteine thiolate ligands. The nickel is further coordinated by two terminal cysteine ligands in a see-saw geometry, while the Fe center is bound by one carbonyl and two cyanide ligands in pseudo-octahedral coordination. A labile site between the two metal centers allows substrate binding (**Figure 1**). The three strong-field ligands impose a low spin state on the iron center, which remains divalent across all isolable states, while the π-donating thiolate ligands on the nickel center suggest the possibility of high-spin or spin-crossover states.[12–14] A series of conserved residues in the secondary coordination sphere have been shown to be critical for catalysis, with orthogonal gas channels and iron-sulfur clusters facilitating the movement of substrates and electrons. Finally, carefully tuned interfaces interact with specific protein partners to delineate the different classes and physiological roles of [NiFe] H_2ase.[15]

The catalytic mechanism of the [NiFe] H_2ase has been probed using diverse electrochemical and spectroscopic techniques across a large, international effort (**Figure 2A**), ranging from Fourier-transform infrared (FTIR) spectroscopy on the Fe-bound diatomics to electron paramagnetic resonance (EPR) spectroscopy on the nickel site to Fe-selective nuclear resonance vibrational spectroscopy (NRVS). The EPR-silent Ni^{II}-Fe^{II} resting state, called Ni-SI_a,[16] undergoes

stepwise proton-coupled reduction to form the Ni-L state, which features a Ni^{I}-Fe^{II} center with a metal-metal bond and a putative protonated cysteine ligand.[18] Pioneering work by the Vincent lab demonstrated the catalytic intermediacy of the Ni-L species utilizing an *in situ* technique combining protein film electrochemistry with attenuated total reflectance infrared spectroscopy (PFIRE).[17] Formal tautomerization of the Ni-L state generates the Ni-C state, with a Ni^{III}(μ-H)Fe^{II} site.[19] Another proton-coupled electron transfer step results in formation of the Ni^{II}(μ-H)Fe^{II} Ni-R state, which can heterolytically release H_2 gas.[3,20] While there has been extensive and elegant work done to characterize each of these intermediates,[21] key elements are still debated, including the catalytic competence of a protonated cysteine ligand, the role of a second-sphere arginine residue, rate-limiting proton transfer steps, the nickel spin state(s), and the role of the strictly-conserved [$Fe^{II}(CN)_2(CO)$] fragment, which remains redox-inert throughout catalysis yet requires a costly biosynthetic process for proper assembly and insertion.[22,23]

The organometallic active site of the [NiFe] H_2ase has inspired a vast and elegant set of synthetic models that reproduce both structural and spectroscopic aspects of this enzyme.[24–26] However, the focus here will be centered around models that reproduce the catalytic nickel site within protein scaffolds.[29] Protein-based models provide biologically relevant ligands and a secondary coordination sphere around the active site, offer the ability to install complexity and asymmetry through rational design, and enable study in aqueous solution for direct comparison to the native enzyme.[27,28,30,31] The nickel-substituted rubredoxin (NiRd) model utilizes a Ni^{II} ion installed within the pseudo-tetrahedral, tetrathiolate iron binding site, reproducing the primary coordination sphere of the nickel in the [NiFe] H_2ase.[32] The NiRd system has been shown to be a functional H_2ase model, with electrocatalytic rates and mechanism that closely resemble those proposed for the native enzyme (**Figure 2B**).[33] The establishment of a mechanistic mimic suggests biochemical precedence for the catalytic relevance of such intermediates within H_2ase.[34]

For example, the NiRd resting state, which contains a high-spin nickel center, can be considered analogous to the Ni-SI_a state[35] while the lack of an arginine residue in the secondary coordination sphere of NiRd supports the competence of a Ni^{I}-SH species to promote hydride formation and ultimately H_2 evolution.[34] While the rates of catalysis by NiRd are high, H_2 evolution requires an overpotential of ~560 mV, which is significantly larger than the negligible (<<100 mV) overpotential observed in catalysis by the native enzyme. Differences in the catalytic overpotential for reduction from Ni^{II} to Ni^{I} likely arise from distinctions in active site geometry, as the [NiFe] H_2ase has a distorted see-saw structure while Ni^{II}Rd is a distorted tetrahedron.[35] Finally, a series of mutant proteins was designed that retained the active site ligation but introduced targeted residues into the secondary coordination sphere, mimicking those seen in the native enzyme.[36]

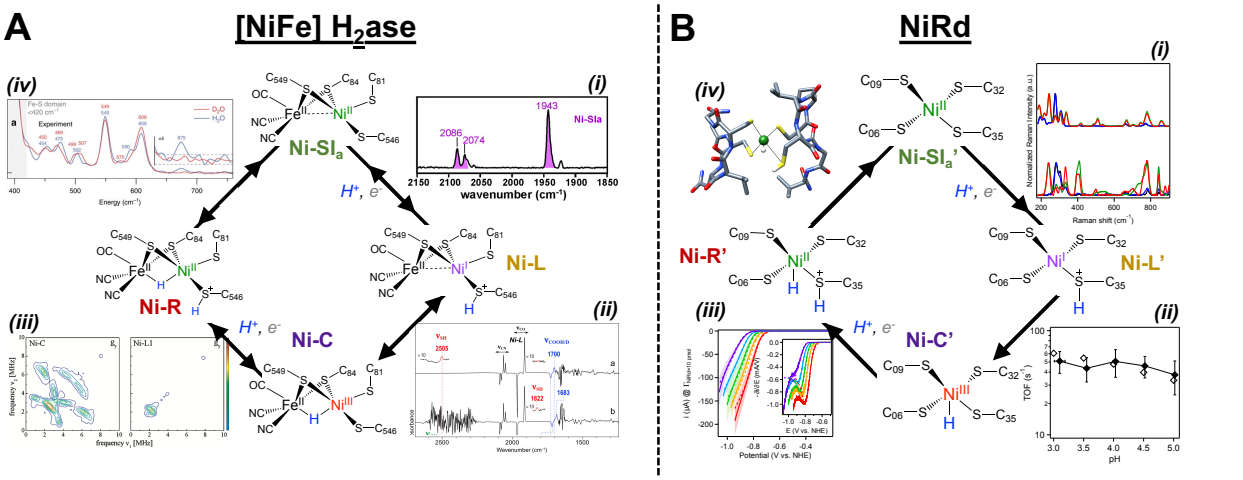

Figure 2. Catalytic mechanisms and primary evidence supporting the proposed intermediate structures for (**A**) [NiFe] hydrogenase and (**B**) nickel-substituted rubredoxin. **A:** (***i***) Spectroelectrochemical FTIR study of *Desulfovibrio vulgaris* Miyazaki F [NiFe] H_2ase showing the Ni-SI_a state (adapted from Ref. 21); (***ii***) Light-induced difference FTIR spectroscopy directly revealing ν(S-H) in the Ni-L state (adapted from Ref. 18); (***iii***) pulsed X-band EPR hyperfine sublevel correlation (HYSCORE) spectroscopy of the Ni-C and Ni-L1 states showing pronounced ridges from the isotopically-labelled $Ni^{III}(\mu\text{-}^{2}H)Fe^{II}$ species that are absent in the photoinduced Ni-L1 state (adapted from Ref. 19); (***iv***) NRVS showing isotopically sensitive bands of the Ni-R state assigned to the $\delta(Ni^{II}(\mu\text{-}H)Fe^{II})$ motion (adapted from Ref. 20). **B:** (***i***) Experimental and calculated multiwavelength resonance Raman spectroscopy on the Ni-SI_a' state of NiRd (adapted from Ref. 35); (***ii***) Experimental and calculated turnover frequencies obtained from quantitative protein film electrochemistry techniques as a function of pH indicative of intramolecular rate-determining proton transfer (adapted from Ref. 34); (***iii***) Simulated electrochemical voltammograms and voltammogram derivatives resolving electrocatalytic mechanism for H^+ reduction by NiRd (adapted from Ref. 34); (***iv***) DFT-calculated structure of the proposed Ni^{II}-H, $C_{35}SH$ (Ni-R') species implicated as the final intermediate prior to heterolytic release of H_2 (adapted from Ref. 34).

These mutations induced dramatic changes in catalytic rates with negligible increases in onset potential, in stark contrast to the conventional trade-off between log(rate) and overpotential often seen for synthetic molecular systems (**Figure 3**).[37] The catalytic behavior of NiRd and, correspondingly, the [NiFe] H_2ase suggest that overcoming traditional catalytic scaling relationships between turnover frequency (TOF) and overpotential may be the result of decoupling dynamical behavior from electronic structure.

In addition to the NiRd metalloprotein system, a similar strategy for constructing H_2ase models was employed by the Chakraborty group, who converted a copper binding protein with a tetracysteinate site to bind nickel.[38] Unlike NiRd, this system appears to use a square planar, low-spin nickel site, analogous to synthetic Ni(II) compounds. Perhaps due to this distinction, the electrocatalytic wave shapes are more similar to those seen for synthetic models than for those observed for NiRd and [NiFe] H_2ase,[34,39] hinting at the role of spin state in the native enzyme. The development of protein-based models of [NiFe] H_2ase provides an opportunity to distinguish how the protein scaffold and local environment control active site structure and spin state to modulate catalysis. Moreover, we anticipate future work will be aimed at installing an $[Fe(CN)_2(CO)]$ center within the biochemical models, exactly

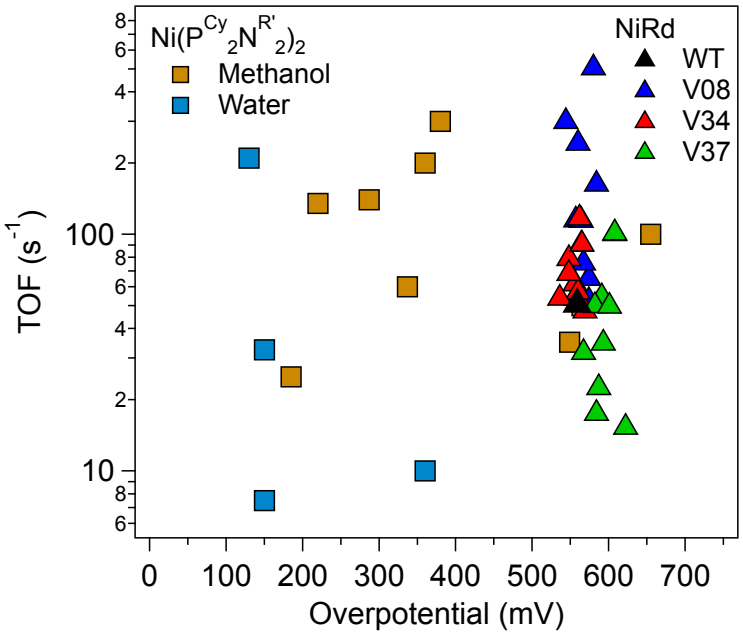

Figure 3. Turnover frequency (TOF) vs. overpotential of Ni($P^{Cy}_2N^{R'}_2$) complexes for H_2 oxidation catalysis and proton reduction by NiRd variants with mutations at the indicated positions (pH 4.0). The typical linear relationship between log(TOF) and overpotential is absent in the NiRd mutant proteins. Data adapted from Ref. 36.

reproducing the structure of the entire [NiFe] H_2ase active site. These efforts, if successful, will ultimately be able to disentangle the role of the iron fragment in the native enzyme.

Carbon monoxide dehydrogenase: Perfect selectivity among a sea of potential products

The reduction of CO_2 to CO is a two-electron, two-proton process with a reduction potential of -520 mV vs. NHE at pH 7. This is sufficient driving force to enable parasitic proton reduction, which is often seen during CO_2 reduction by many synthetic and materials-based catalysts.[40] However, biological systems are able to avoid these side reactions through the combination of electronic, structural, and environmental control.[41] The carbon monoxide dehydrogenase exemplifies this control, demonstrating rapid and reversible CO_2/CO interconversion with no evidence for formation of H_2, formic acid/formate, or other C_{2+} coupled products.[42]

The active site of CODH, denoted the C cluster, features a non-canonical [$NiFe_4S_4$] cluster (**Figure 1**).[43] The cubane subsite is linked to the protein through 4 cysteine ligands, and an exogenous Fe center, often denoted Fe_u, is coordinated by an additional cysteine as well as a histidine residue. Fe_u is connected to the cubane through one of the sulfide ligands, which mediates antiferromagnetic exchange between the two subsites of the C cluster.[44] While there are now many representative X-ray crystal structures of CODH in reduced, CO_2-bound, and inhibited forms as well as electrochemical and activity assay data, the CO-bound form has been inaccessible due to the high activity of CODH towards CO oxidation. Moreover, it has not been possible to resolve the individual oxidation and spin states on each metal center in any of the isolable states.[44] Thus, an experimentally validated, mechanistic understanding of CO_2 reduction and CO oxidation by CODH is lacking.

Protein-based models have provided complementary insight towards understanding the mechanism and selectivity of native CODH. Preceding publication of the CODH crystal structure, a [$NiFe_3S_4$] cluster was incorporated within the *Pyrococcus furiosus (Pf)* and *Desulfovibrio gigas* (*Dg*) ferredoxin (Fd) proteins and characterized using EPR and Mössbauer spectroscopy.[45] An S

= 3/2 spin state was found for the reduced $[NiFe_3S_4]^+$ Fd cluster, which, in light of subsequent structural information, likely represents the spin state of the C cluster cubane subsite.[46] Beyond replicating the subsite electronic structure, recent work reveals that the $[NiFe_3S_4]$ *Pf* Fd is capable of reversible electron transfer as well as binding of cyanide, a CODH inhibitor, and binding of carbon monoxide, a CODH substrate.[47] That CO binding can occur, but oxidative conversion cannot, implicates the nickel center as the substrate carbon binding site (**Figure 4A**). Moreover, the canonical $[Fe_4S_4]$ *Pf* Fd is inert towards CO binding, suggesting the subtle electronic structure differences between a Ni^{II} and Fe^{II} ion underlie the integration of nickel into the active site cubane. The continued development and spectroscopic characterization of the $[NiFe_3S_4]$ *Pf* Fd system as a protein-based model of CODH is likely to yield great insight into the specific roles of the cluster subsite and, by extension, the Fe_u center, towards substrate binding, conversion, and reaction selectivity.[47]

A different, semisynthetic protein-based model has provided information on additional factors that contribute to enzymatic selectivity. Specifically, the incorporation of a nickel(II) cyclam catalyst into an azurin protein scaffold via axial histidine ligation increased the selectivity for photodriven CO production over H^+ reduction by a factor of 20.[48] Further enhancement was conferred by including an additional redox-active metal in close proximity, and systems in which a photosensitizer was directly attached to the protein scaffold exhibited complete selectivity for light-driven CO_2 reduction to CO.[49] In another report, a Ni(II) terpy catalyst was attached to an engineered photosensitizer protein, showing high turnover numbers for CO production.[50] In both cases, catalysis is significantly slower than in the native enzyme, though direct comparison of rates and catalytic overpotentials is challenging because identical measurement conditions cannot be accessed across the three systems. The CODH models demonstrate that active site electronic structure, secondary coordination sphere, and long range electron transfer rates all impact selectivity, implicating the presence of analogous multiscale contributions in native CODH.

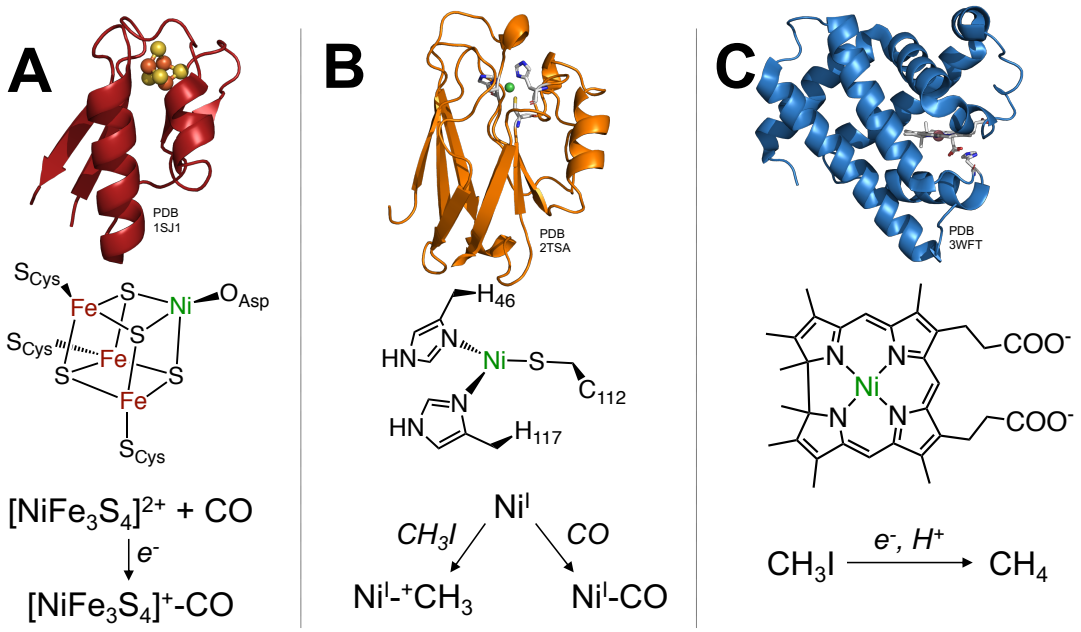

Figure 4. Model protein and active-site structures for (**A**) $[NiFe_3S_4]$ *Pyrococcus furiosus* ferredoxin as a model of CODH; (**B**) nickel-substituted M121A *Pseudomonas aeruginosa* azurin as a model of ACS; (**C**) tetradehydrocorrin-bound *Equus caballus* myoglobin as a model for MCR. The demonstrated reactivity of the models that mimics that of the native enzymes is shown along the bottom.

Acetyl coenzyme A synthase: Nature's organometallic catalyst

The reaction catalyzed by ACS is directly analogous to synthetic organometallic processes: A cationic methyl group, donated by a cobalt corrinoid protein, binds to the nickel center through an oxidative addition process. Carbon monoxide inserts into the metal-methyl bond, and the resultant acyl group is transferred to the thiol of coenzyme A, forming a thioester through reductive thiolysis.[53] This reaction represents the cornerstone step in the Wood-Ljungdahl pathway, which is the primary metabolic process in diverse anaerobic bacteria and archaea.[53] Despite the significance of this reaction, great debate persists over the basic catalytic mechanism of ACS, including the sites and sequence of substrate binding, relevant oxidation states and electronic structures, and electron and proton requirements.[54–56] Fueling the dispute are conflicting observations between the native enzyme, which appears to utilize a $Ni^{III/I}$ transition,[57] and synthetic mimics, which require a Ni^0 state for two-electron methyl addition and CO insertion.[58,59]

While a biological Ni^0 site has yet to be identified,[60] reactivity metrics had suggested it may be necessary to reconcile all of the experimental observations about ACS.

A protein-based model of ACS has the potential to settle this debate. The model, based on a nickel-substituted M121A variant of the *Pseudomonas aeruginosa* azurin (NiAz) protein, shares many electronic features and reactivity traits with ACS, demonstrating the capacity of a biological nickel center to support nucleophilic methyl transfer and favoring the relevance of the $Ni^{II/I}$ couple for ACS catalysis (**Figure 4B**). Detailed electronic structure analysis using pulsed EPR spectroscopy reveals the importance of a distorted trigonal site, analogous to that observed in ACS, for weak CO affinity, which prevents enzymatic inhibition.[61] In addition, an EPR-active, S = ½ Ni-CH_3 Az species was isolated and shown to possess an "inverted ligand field", in which the metal remained a physically d^9, Ni^I center, necessitating a cationic Z-type methyl ligand.[61,62] An analogous electronic structure is implicated in the elusive S = ½ Ni-CH_3 ACS state, which is thought to prevent degradative reductive elimination between the bound methyl group and a cysteine thiolate ligand.[63,64] Thus, the NiAz-based ACS model has not only uncovered a biochemically feasible catalytic mechanism, it has allowed access to previously inaccessible intermediates, revealing strategies that nature has employed for effective catalysis and enzyme stability.

Methyl coenzyme M reductase: Fueling the ocean floor

MCR is responsible both for the generation and anaerobic oxidation of methane, which drives energy conservation in the anaerobic methanotrophic archaea (ANME).[65] MCR breaks one of the strongest C-H bonds known (104 kcal/mol), putatively through a radical activation pathway.[67] At the active site of MCR lies the most reduced tetrapyrrole cofactor found in nature, coenzyme F430, which is highly air-sensitive and requires a multi-step biosynthetic process (**Figure 1**).[68,69] As the excessive release of this greenhouse gas into the atmosphere from commercial livestock operations and natural gas fracturing sites presents an urgent threat, there is great interest in

reproducing the methane oxidation capability of MCR in a robust scaffold, with potential for broad and rapid deployment.

It has been known for many decades that extraction and isolation of coenzyme F430 does not result in an active catalyst for methane production or oxidation under physiologically relevant conditions. On the other hand, MCR-like reactivity is observed in a protein-based model of MCR, which features a nickel tetradehydrocorrin macrocycle (Ni(TDHC)) integrated into apo-myoglobin (Mb) (**Figure 4C**). The Ni(TDHC)-Mb shows selective methane generation and reductive dehalogenation under mild aqueous conditions, though the turnover numbers are significantly lower than those of the native enzyme.[71] In the isolated Ni(TDHC) controls, no products are observed, pointing to a direct role of the Mb scaffold in modulating the catalytic activity. Interestingly, no ethane is generated, consistent with a two-electron rather than a radical catalytic mechanism.[72] Further development of the MCR reactivity of this system using biologically relevant substrates will enable more significant mechanistic parallels between the model and native enzymes to be drawn.

Conclusions and Outlook

The field of artificial metalloenzymes presents many opportunities for today's chemist, with the potential to discover new-to-nature reactions, enhance rates or selectivity for natural processes, and deconstruct elementary contributors towards enzymatic catalysis. The native enzymes and model systems discussed herein are intended to illustrate the mechanistic insight that can be obtained from studying protein-based models, which may ultimately lead to functional models that recapitulate key enzymatic features. Considering the diversity of reactions performed across all of the nickel metalloenzymes, interest in both understanding and replicating these processes is highly likely to increase as applications to energy and environment are explored.

Acknowledgements

The model hydrogenase work in the Shafaat lab is supported by the National Science Foundation (CHE-1454289, CHE-2108684), while the model CODH and ACS work in the Shafaat lab is supported by the Department of Energy (DE-SC0018020). Early research on novel CODH models was supported by the Alfred P. Sloan Foundation (FG-2018-10837).

References

(1) Alfano, M.; Cavazza, C. Structure, function, and biosynthesis of nickel-dependent enzymes. *Protein Science* **2020**, *29*, 1071–1089 DOI: 10.1002/pro.3836.

(2) Jeoung, J.-H.; Nianios, D.; Fetzner, S.; Dobbek, H. Quercetin 2,4-Dioxygenase Activates Dioxygen in a Side-On O_2–Ni Complex. *Angew. Chem. Int. Ed.* **2016**, *55*, 3281–3284 DOI: 10.1002/anie.201510741.

* The first structural characterization of nickel-bound quercetin dioxygenase. This structure also shows the mode of coordination of O_2 to the metal center.

(3) Ogata, H.; Nishikawa, K.; Lubitz, W. Hydrogens detected by subatomic resolution protein crystallography in a [NiFe] hydrogenase. *Nature* **2015**, *520*, 571–574 DOI: 10.1038/nature14110.

** This ultra-high resolution crystal structure confirmed the structure of the most reduced, Ni-R state of the [NiFe] hydrogenase.

(4) Fesseler, J.; Jeoung, J.-H.; Dobbek, H. How the [$NiFe_4S_4$] Cluster of CO Dehydrogenase Activates CO_2 and NCO−. *Angew. Chem. Int. Ed.* **2015**, *54*, 8560–8564 DOI: 10.1002/anie.201501778.

(5) Doukov, T. I.; Iverson, T. M.; Seravalli, J.; Ragsdale, S. W.; Drennan, C. L. A Ni-Fe-Cu Center in a Bifunctional Carbon Monoxide Dehydrogenase/ Acetyl-CoA Synthase. *Science* **2002**, *298*, 567–572 DOI: 10.1126/science.1075843.

(6) Darnault, C.; Volbeda, A.; Kim, E. J.; Legrand, P.; Vernède, X.; Lindahl, P. A.; Fontecilla-Camps, J. C. Ni-Zn-[Fe_4-S_4] and Ni-Ni-[Fe_4-S_4] clusters in closed and open α subunits of acetyl-CoA synthase/carbon monoxide dehydrogenase. *Nature Structural Biology* **2003**, *10*, 271–279 DOI: 10.1038/nsb912.

(7) Cedervall, P. E.; Dey, M.; Pearson, A. R.; Ragsdale, S. W.; Wilmot, C. M. Structural Insight into Methyl-Coenzyme M Reductase Chemistry Using Coenzyme B Analogues,. *Biochemistry* **2010**, *49*, 7683–7693 DOI: 10.1021/bi100458d.

(8) Desguin, B.; Goffin, P.; Viaene, E.; Kleerebezem, M.; Martin-Diaconescu, V.; Maroney, M. J.; Declercq, J.-P.; Soumillion, P.; Hols, P. Lactate racemase is a nickel-dependent enzyme activated by a widespread maturation system. *Nat Commun* **2014**, *5*, 3615 DOI: 10.1038/ncomms4615.

(9) Barondeau, D. P.; Kassmann, C. J.; Bruns, C. K.; Tainer, J. A.; Getzoff, E. D. Nickel Superoxide Dismutase Structure and Mechanism. *Biochemistry* **2004**, *43*, 8038–8047 DOI: 10.1021/bi0496081.

(10) He, M. M.; Clugston, S. L.; Honek, J. F.; Matthews, B. W. Determination of the Structure of *Escherichia coli* Glyoxalase I Suggests a Structural Basis for Differential Metal Activation. *Biochemistry* **2000**, *39*, 8719–8727 DOI: 10.1021/bi000856g.

(11) Pochapsky, T. C.; Pochapsky, S. S.; Ju, T.; Hoefler, C.; Liang, J. A Refined Model for the Structure of Acireductone Dioxygenase from *Klebsiella ATCC 8724* Incorporating Residual Dipolar Couplings. *J Biomol NMR* **2006**, *34*, 117–127 DOI: 10.1007/s10858-005-5735-8.

(12) Kaliakin, D. S.; Zaari, R. R.; Varganov, S. A. Effect of H_2 Binding on the Nonadiabatic Transition Probability between Singlet and Triplet States of the [NiFe]-Hydrogenase Active Site. *J. Phys. Chem. A* **2015**, *119*, 1066–1073 DOI: 10.1021/jp510522z.

(13) Dong, G.; Ryde, U.; Jensen, H. J. A.; Hedegård, E. D. Exploration of H_2 binding to the [NiFe]-hydrogenase active site with multiconfigurational density functional theory. *Phys. Chem. Chem. Phys.* **2018**, *20*, 794–801 DOI: 10.1039/C7CP06767D.

(14) Breglia, R.; Greco, C.; Fantucci, P.; De Gioia, L.; Bruschi, M. Reactivation of the Ready and Unready Oxidized States of [NiFe]-Hydrogenases: Mechanistic Insights from DFT Calculations. *Inorg. Chem.* **2019**, *58*, 279–293 DOI: 10.1021/acs.inorgchem.8b02348.

(15) Greening, C.; Biswas, A.; Carere, C. R.; Jackson, C. J.; Taylor, M. C.; Stott, M. B.; Cook, G. M.; Morales, S. E. Genomic and metagenomic surveys of hydrogenase distribution indicate H_2 is a widely utilised energy source for microbial growth and survival. *The ISME Journal* **2016**, *10*, 761–777 DOI: 10.1038/ismej.2015.153.

** A large-scale metagenomic survey reclassifying and ordering all hydrogenases by gene cluster, metal binding motifs, and phylogeny.

(16) de Lacey, A. L.; Hatchikian, E. C.; Volbeda, A.; Frey, M.; Fontecilla-Camps, J. C.; Fernandez, V. M. Infrared-Spectroelectrochemical Characterization of the [NiFe] Hydrogenase of *Desulfovibrio gigas*. *J. Am. Chem. Soc.* **1997**, *119*, 7181–7189 DOI: 10.1021/ja963802w.

(17) Hidalgo, R.; Ash, P. A.; Healy, A. J.; Vincent, K. A. Infrared Spectroscopy During Electrocatalytic Turnover Reveals the Ni-L Active Site State During H_2 Oxidation by a NiFe Hydrogenase. *Angew. Chem. Int. Ed.* **2015**, *54*, 7110–7113 DOI: 10.1002/anie.201502338.

** This work used *in situ* FT-IR spectroelectrochemistry to provide the first experimental evidence that the Ni-L state is observed under turnover conditions and thus is catalytically relevant.

(18) Tai, H.; Nishikawa, K.; Higuchi, Y.; Mao, Z.; Hirota, S. Cysteine SH and Glutamate COOH Contributions to [NiFe] Hydrogenase Proton Transfer Revealed by Highly Sensitive FTIR Spectroscopy. *Angewandte Chemie International Edition* **2019**, *58*, 13285–13290 DOI: 10.1002/anie.201904472.

(19) Brecht, M.; van Gastel, M.; Buhrke, T.; Friedrich, B.; Lubitz, W. Direct detection of a hydrogen ligand in the [NiFe] center of the regulatory H_2-sensing hydrogenase from

Ralstonia eutropha in its reduced state by HYSCORE and ENDOR spectroscopy. *J. Am. Chem. Soc.* **2003**, *125*, 13075–13083 DOI: 10.1021/ja036624x.

* Pulsed EPR spectroscopy was used to provide the first experimental evidence for a metal hydride species within a biological system.

(20) Ogata, H.; Krämer, T.; Wang, H.; Schilter, D.; Pelmenschikov, V.; van Gastel, M.; Neese, F.; Rauchfuss, T. B.; Gee, L. B.; Scott, A. D.; et al. Hydride bridge in [NiFe]-hydrogenase observed by nuclear resonance vibrational spectroscopy. *Nat. Commun.* **2015**, *6*, 7890 DOI: 10.1038/ncomms8890.

(21) Lubitz, W.; Ogata, H.; Rüdiger, O.; Reijerse, E. Hydrogenases. *Chem. Rev.* **2014**, *114*, 4081–4148 DOI: 10.1021/cr4005814.

(22) Lacasse, M. J.; Zamble, D. B. [NiFe]-Hydrogenase Maturation. *Biochemistry* **2016**, *55*, 1689–1701 DOI: 10.1021/acs.biochem.5b01328.

(23) Roncaroli, F.; Bill, E.; Friedrich, B.; Lenz, O.; Lubitz, W.; Pandelia, M.-E. Cofactor composition and function of a H_2-sensing regulatory hydrogenase as revealed by Mössbauer and EPR spectroscopy. *Chem. Sci.* **2015**, *6*, 4495–4507 DOI: 10.1039/C5SC01560J.

(24) Weber, K.; Krämer, T.; Shafaat, H. S.; Weyhermuller, T.; Bill, E.; van Gastel, M.; Neese, F.; Lubitz, W. A functional [NiFe]-hydrogenase model compound that undergoes biologically relevant reversible thiolate protonation. *J. Am. Chem. Soc.* **2012**, *134*, 20745–20755 DOI: 10.1021/ja309563p.

* Presentation of a new class of synthetic model of the [NiFe] hydrogenase that undergoes protonation of a terminal thiolate residue, analogous to the native enzyme.

(25) Yang, X.; Elrod, L. C.; Reibenspies, J. H.; Hall, M. B.; Darensbourg, M. Y. Oxygen uptake in complexes related to [NiFeS]- and [NiFeSe]-hydrogenase active sites. *Chem. Sci.* **2019**, *10*, 1368–1373 DOI: 10.1039/C8SC04436H.

(26) Brazzolotto, D.; Wang, L.; Tang, H.; Gennari, M.; Queyriaux, N.; Philouze, C.; Demeshko, S.; Meyer, F.; Orio, M.; Artero, V.; et al. Tuning Reactivity of Bioinspired [NiFe]-Hydrogenase Models by Ligand Design and Modeling the CO Inhibition Process. *ACS Catal.* **2018**, *8*, 10658–10667 DOI: 10.1021/acscatal.8b02830.

(27) DiPrimio, D. J.; Holland, P. L. Repurposing metalloproteins as mimics of natural metalloenzymes for small-molecule activation. *J. Inorg. Biochem.* **2021**, *219*, 111430 DOI: 10.1016/j.jinorgbio.2021.111430.

(28) Jeong, W. J.; Yu, J.; Song, W. J. Proteins as diverse, efficient, and evolvable scaffolds for artificial metalloenzymes. *Chem. Commun.* **2020**, *56*, 9586–9599 DOI: 10.1039/D0CC03137B.

(29) Dutta, A.; DuBois, D. L.; Roberts, J. A. S.; Shaw, W. J. Amino acid modified Ni catalyst exhibits reversible H_2 oxidation/production over a broad pH range at elevated temperatures. *PNAS* **2014**, *111*, 16286–16291 DOI: 10.1073/pnas.1416381111.

(30) Rodriguez-Maciá, P.; Dutta, A.; Lubitz, W.; Shaw, W. J.; Rüdiger, O. Direct Comparison of the Performance of a Bio-inspired Synthetic Nickel Catalyst and a [NiFe]-Hydrogenase, Both Covalently Attached to Electrodes. *Angew. Chem. Int. Ed.* **2015**, *54*, 12303–12307 DOI: 10.1002/anie.201502364.

(31) Klug, C. M.; Cardenas, A. J. P.; Bullock, R. M.; O'Hagan, M.; Wiedner, E. S. Reversing the Tradeoff between Rate and Overpotential in Molecular Electrocatalysts for H_2 Production. *ACS Catal.* **2018**, *8*, 3286–3296 DOI: 10.1021/acscatal.7b04379.

(32) Slater, J. W.; Shafaat, H. S. Nickel-Substituted Rubredoxin as a Minimal Enzyme Model for Hydrogenase. *J. Phys. Chem. Lett.* **2015**, *6*, 3731–3736 DOI: 10.1021/acs.jpclett.5b01750.

(33) Léger, C.; Jones, A. K.; Roseboom, W.; Albracht, S. P. J.; Armstrong, F. A. Enzyme Electrokinetics: Hydrogen Evolution and Oxidation by *Allochromatium vinosum* [NiFe]-Hydrogenase†. *Biochemistry* **2002**, *41*, 15736–15746 DOI: 10.1021/bi026586e.

(34) Slater, J. W.; Marguet, S. C.; Monaco, H. A.; Shafaat, H. S. Going beyond Structure: Nickel-Substituted Rubredoxin as a Mechanistic Model for the [NiFe] Hydrogenases. *J. Am. Chem. Soc.* **2018**, *140*, 10250–10262 DOI: 10.1021/jacs.8b05194.

** A comprehensive electrochemical and computational analysis of the electrocatalytic proton reduction activity of nickel-substituted rubredoxin, a protein-based hydrogenase model with biologically relevant active site coordination.

(35) Slater, J. W.; Marguet, S. C.; Cirino, S. L.; Maugeri, P. T.; Shafaat, H. S. Experimental and DFT Investigations Reveal the Influence of the Outer Coordination Sphere on the Vibrational Spectra of Nickel-Substituted Rubredoxin, a Model Hydrogenase Enzyme. *Inorg. Chem.* **2017**, *56*, 3926–3938 DOI: 10.1021/acs.inorgchem.6b02934.

(36) Slater, J. W.; Marguet, S. C.; Gray, M. E.; Monaco, H. A.; Sotomayor, M.; Shafaat, H. S. Power of the Secondary Sphere: Modulating Hydrogenase Activity in Nickel-Substituted Rubredoxin. *ACS Catal.* **2019**, *9*, 8928–8942 DOI: 10.1021/acscatal.9b01720.

(37) Pegis, M. L.; McKeown, B. A.; Kumar, N.; Lang, K.; Wasylenko, D. J.; Zhang, X. P.; Raugei, S.; Mayer, J. M. Homogenous Electrocatalytic Oxygen Reduction Rates Correlate with Reaction Overpotential in Acidic Organic Solutions. *ACS Cent. Sci.* **2016**, *2*, 850–856 DOI: 10.1021/acscentsci.6b00261.

(38) Selvan, D.; Prasad, P.; Farquhar, E. R.; Shi, Y.; Crane, S.; Zhang, Y.; Chakraborty, S. Redesign of a Copper Storage Protein into an Artificial Hydrogenase. *ACS Catal.* **2019**, *9*, 5847–5859 DOI: 10.1021/acscatal.9b00360.

(39) Léger, C.; Jones, A. K.; Albracht, S. P. J.; Armstrong, F. A. Effect of a Dispersion of Interfacial Electron Transfer Rates on Steady State Catalytic Electron Transport in [NiFe]-

hydrogenase and Other Enzymes. *J. Phys. Chem. B* **2002**, *106*, 13058–13063 DOI: 10.1021/jp0265687.

(40) Barlow, J. M.; Yang, J. Y. Thermodynamic Considerations for Optimizing Selective CO_2 Reduction by Molecular Catalysts. *ACS Cent. Sci.* **2019**, *5*, 580–588 DOI: 10.1021/acscentsci.9b00095.

(41) Shafaat, H. S.; Yang, J. Y. Uniting Biological and Chemical Strategies for Selective CO_2 Reduction. *Nat. Catalysis* **2021***, in press*.

(42) Wang, V. C.-C.; Islam, S. T. A.; Can, M.; Ragsdale, S. W.; Armstrong, F. A. Investigations by Protein Film Electrochemistry of Alternative Reactions of Nickel-Containing Carbon Monoxide Dehydrogenase. *J. Phys. Chem. B* **2015**, *119*, 13690–13697 DOI: 10.1021/acs.jpcb.5b03098.

** This quantitative electrochemical study was coupled with gas chromatography and NMR spectroscopy to reveal negligible amounts of either formate or H_2 produced by CODH even at high driving force, confirming the strict enzymatic selectivity for reducing CO_2 to CO.

(43) Drennan, C. L.; Heo, J.; Sintchak, M. D.; Schreiter, E.; Ludden, P. W. Life on carbon monoxide: X-ray structure of *Rhodospirillum rubrum* Ni-Fe-S carbon monoxide dehydrogenase. *PNAS* **2001**, *98*, 11973–11978 DOI: 10.1073/pnas.211429998.

(44) Hu, Z.; Spangler, N. J.; Anderson, M. E.; Xia, J.; Ludden, P. W.; Lindahl, P. A.; Münck, E. Nature of the C-Cluster in Ni-Containing Carbon Monoxide Dehydrogenases. *J. Am. Chem. Soc.* **1996**, *118*, 830–845 DOI: 10.1021/ja9528386.

(45) Conover, R. C.; Park, J. B.; Adams, M. W. W.; Johnson, M. K. Formation and properties of an iron-nickel sulfide ($NiFe_3S_4$) cluster in *Pyrococcus furiosus* ferredoxin. *J. Am. Chem. Soc.* **1990**, *112*, 4562–4564 DOI: 10.1021/ja00167a074.

(46) Srivastava, K. K. P.; Surerus, K. K.; Conover, R. C.; Johnson, M. K.; Park, J. B.; Adams, M. W. W.; Munck, E. Moessbauer study of zinc-iron-sulfur $ZnFe_3S_4$ and nickel-iron-sulfur

$NiFe_3S_4$ clusters in *Pyrococcus furiosus* ferredoxin. *Inorg. Chem.* **1993**, *32*, 927–936 DOI: 10.1021/ic00058a029.

(47) Lewis, L.; Shafaat, H. Reversible electron transfer and substrate binding support [$NiFe_3S_4$] ferredoxin as a protein-based model for [NiFe] carbon monoxide dehydrogenase. *Inorg. Chem.* **2021**.

(48) Schneider, C. R.; Shafaat, H. S. An internal electron reservoir enhances catalytic CO_2 reduction by a semisynthetic enzyme. *Chem. Commun.* **2016**, *52*, 9889–9892 DOI: 10.1039/C6CC03901D.

(49) Schneider, C. R.; Manesis, A. C.; Stevenson, M. J.; Shafaat, H. S. A photoactive semisynthetic metalloenzyme exhibits complete selectivity for CO_2 reduction in water. *Chem. Commun.* **2018**, *54*, 4681–4684 DOI: 10.1039/C8CC01297K.

(50) Liu, X.; Kang, F.; Hu, C.; Wang, L.; Xu, Z.; Zheng, D.; Gong, W.; Lu, Y.; Ma, Y.; Wang, J. A genetically encoded photosensitizer protein facilitates the rational design of a miniature photocatalytic CO_2 -reducing enzyme. *Nature Chemistry* **2018**, *10*, 1201–1206 DOI: 10.1038/s41557-018-0150-4.

(51) Dobbek, H.; Svetlitchnyi, V.; Gremer, L.; Huber, R.; Meyer, O. Crystal Structure of a Carbon Monoxide Dehydrogenase Reveals a [Ni-4Fe-5S] Cluster. *Science* **2001**, *293*, 1281–1285 DOI: 10.1126/science.1061500.

(52) Tasker, S. Z.; Standley, E. A.; Jamison, T. F. Recent advances in homogeneous nickel catalysis. *Nature* **2014**, *509*, 299–309 DOI: 10.1038/nature13274.

(53) Ragsdale, S. W. Biological Carbon Fixation by an Organometallic Pathway: Evidence Supporting the Paramagnetic Mechanism of the Nickel-Iron-Sulfur Acetyl-CoA Synthase. In *Comprehensive Coordination Chemistry III*; Elsevier, 2021; pp 611–633.

(54) Can, M.; Giles, L. J.; Ragsdale, S. W.; Sarangi, R. X-ray Absorption Spectroscopy Reveals an Organometallic Ni–C Bond in the CO-Treated Form of Acetyl-CoA Synthase. *Biochemistry* **2017**, *56*, 1248–1260 DOI: 10.1021/acs.biochem.6b00983.

(55) James, C. D.; Wiley, S.; Ragsdale, S. W.; Hoffman, B. M. ^{13}C Electron Nuclear Double Resonance Spectroscopy Shows Acetyl-CoA Synthase Binds Two Substrate CO in Multiple Binding Modes and Reveals the Importance of a CO-Binding "Alcove." *J. Am. Chem. Soc.* **2020**, *142*, 15362–15370 DOI: 10.1021/jacs.0c05950.

* Pulsed EPR study on ACS highlighting the necessity of a hydrophobic, polarizable cavity near the nickel center for enabling CO binding.

(56) Tan, X.; Surovtsev, I. V.; Lindahl, P. A. Kinetics of CO Insertion and Acetyl Group Transfer Steps, and a Model of the Acetyl-CoA Synthase Catalytic Mechanism. *J. Am. Chem. Soc.* **2006**, *128*, 12331–12338 DOI: 10.1021/ja0627702.

(57) Seravalli, J.; Kumar, M.; Ragsdale, S. W. Rapid Kinetic Studies of Acetyl-CoA Synthesis: Evidence Supporting the Catalytic Intermediacy of a Paramagnetic NiFeC Species in the Autotrophic Wood−Ljungdahl Pathway†. *Biochemistry* **2002**, *41*, 1807–1819 DOI: 10.1021/bi011687i.

(58) Yoo, C.; Ajitha, M. J.; Jung, Y.; Lee, Y. Mechanistic Study on C–C Bond Formation of a Nickel(I) Monocarbonyl Species with Alkyl Iodides: Experimental and Computational Investigations. *Organometallics* **2015**, *34*, 4305–4311 DOI: 10.1021/acs.organomet.5b00548.

(59) Ariyananda, P. W. G.; Kieber-Emmons, M. T.; Yap, G. P. A.; Riordan, C. G. Synthetic analogs for evaluating the influence of N–H···S hydrogen bonds on the formation of thioester in acetyl coenzyme A synthase. *Dalton Trans.* **2009**, *0*, 4359–4369 DOI: 10.1039/B901192G.

(60) Lindahl, P. A. Acetyl-coenzyme A synthase: the case for a Ni_p^0-based mechanism of catalysis. *J Biol Inorg Chem* **2004**, *9*, 516–524 DOI: 10.1007/s00775-004-0564-x.

(61) Kisgeropoulos, E. C.; Manesis, A. C.; Shafaat, H. S. Ligand Field Inversion as a Mechanism to Gate Bioorganometallic Reactivity: Investigating a Biochemical Model of

Acetyl CoA Synthase Using Spectroscopy and Computation. *J. Am. Chem. Soc.* **2021**, *143*, 849–867 DOI: 10.1021/jacs.0c10135.

** The first experimental demonstration of an “inverted ligand field” within a biochemical system, establishing precedence for similar motifs to play important roles in native enzymes.

(62) Hoffmann, R.; Alvarez, S.; Mealli, C.; Falceto, A.; Cahill, T. J.; Zeng, T.; Manca, G. From Widely Accepted Concepts in Coordination Chemistry to Inverted Ligand Fields. *Chem. Rev.* **2016**, *116*, 8173–8192 DOI: 10.1021/acs.chemrev.6b00251.

(63) Oderinde, M. S.; Frenette, M.; Robbins, D. W.; Aquila, B.; Johannes, J. W. Photoredox Mediated Nickel Catalyzed Cross-Coupling of Thiols With Aryl and Heteroaryl Iodides via Thiyl Radicals. *J. Am. Chem. Soc.* **2016**, *138*, 1760–1763 DOI: 10.1021/jacs.5b11244.

(64) Schultz, J. W.; Fuchigami, K.; Zheng, B.; Rath, N. P.; Mirica, L. M. Isolated Organometallic Nickel(III) and Nickel(IV) Complexes Relevant to Carbon–Carbon Bond Formation Reactions. *J. Am. Chem. Soc.* **2016**, *138*, 12928–12934 DOI: 10.1021/jacs.6b06862.

(65) Thauer, R. K. Methyl (Alkyl)-Coenzyme M Reductases: Nickel F-430-Containing Enzymes Involved in Anaerobic Methane Formation and in Anaerobic Oxidation of Methane or of Short Chain Alkanes. *Biochemistry* **2019**, *58*, 5198–5220 DOI: 10.1021/acs.biochem.9b00164.

(66) Borrel, G.; Adam, P. S.; McKay, L. J.; Chen, L.-X.; Sierra-García, I. N.; Sieber, C. M. K.; Letourneur, Q.; Ghozlane, A.; Andersen, G. L.; Li, W.-J.; et al. Wide diversity of methane and short-chain alkane metabolisms in uncultured archaea. *Nat Microbiol* **2019**, *4*, 603–613 DOI: 10.1038/s41564-019-0363-3.

(67) Patwardhan, A.; Sarangi, R.; Ginovska, B.; Raugei, S.; Ragsdale, S. W. Nickel–Sulfonate Mode of Substrate Binding for Forward and Reverse Reactions of Methyl-SCoM Reductase Suggest a Radical Mechanism Involving Long-Range Electron Transfer. *J. Am. Chem. Soc.* **2021**, *143*, 5481–5496 DOI: 10.1021/jacs.1c01086.

(68) Zheng, K.; Ngo, P. D.; Owens, V. L.; Yang, X.; Mansoorabadi, S. O. The biosynthetic pathway of coenzyme F430 in methanogenic and methanotrophic archaea. *Science* **2016**, *354*, 339–342 DOI: 10.1126/science.aag2947.

** Full determination of the biosynthetic pathway for the nickel F430 cofactor of methyl coenzyme M reductase.

(69) Moore, S. J.; Sowa, S. T.; Schuchardt, C.; Deery, E.; Lawrence, A. D.; Ramos, J. V.; Billig, S.; Birkemeyer, C.; Chivers, P. T.; Howard, M. J.; et al. Elucidation of the biosynthesis of the methane catalyst coenzyme F430. *Nature* **2017**, *543*, 78–82 DOI: 10.1038/nature21427.

(70) Nayak, D. D.; Liu, A.; Agrawal, N.; Rodriguez-Carerro, R.; Dong, S.-H.; Mitchell, D. A.; Nair, S. K.; Metcalf, W. W. Functional interactions between posttranslationally modified amino acids of methyl-coenzyme M reductase in *Methanosarcina acetivorans*. *PLOS Biology* **2020**, *18*, e3000507 DOI: 10.1371/journal.pbio.3000507.

(71) Oohora, K.; Miyazaki, Y.; Hayashi, T. Myoglobin Reconstituted with Ni Tetradehydrocorrin as a Methane-Generating Model of Methyl-coenzyme M Reductase. *Angew Chem Int Ed Engl* **2019**, *58*, 13813–13817 DOI: 10.1002/anie.201907584.

* First report of a functional protein-based model for MCR, which generates methane from methyl iodide, based on integration of a nickel tetradehydrocorrin cofactor into apo-myoglobin.

(72) Miyazaki, Y.; Oohora, K.; Hayashi, T. Methane Generation and Reductive Debromination of Benzylic Position by Reconstituted Myoglobin Containing Nickel Tetradehydrocorrin as a Model of Methyl-coenzyme M Reductase. *Inorg. Chem.* **2020**, *59*, 11995–12004 DOI: 10.1021/acs.inorgchem.0c00901.